Supporting Information

Thermally Driven Interfacial Switch Between Adhesion and Anti-adhesion on Air Bubbles in Aqueous Media

Ruixiao Wang, [a] Mingchao Wang, [d] Chun Wang, [a] Qinglin Yang, [a] Jingming Wang*[a,b] and Lei Jiang [a,b,c]

a. Key Laboratory of Bio-Inspired Smart Interfacial Science and Technology of Ministry of Education, School of Chemistry, Beihang University, Beijing 100083, China.

b. Beijing Advanced Innovation Center for Biomedical Engineering, Beihang University, Beijing, 100191, China.

c. Laboratory of Bio-inspired Smart Interface Science, Technical Institute of Physics and Chemistry, Chinese Academy of Sciences, Beijing 100190, China

d. Beijing BOE Display Technology Co. Ltd, Beijing 100176, China.

* Corresponding authors: wangjm@buaa.edu.cn (J. M. Wang)

S1 The surface structures of the PNIPAAM/PP composite film

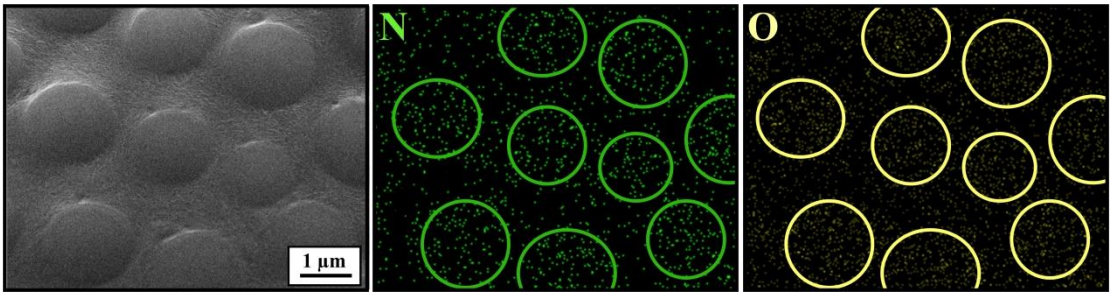

Figure S1 SEM images and EDS mapping of the PNIPAAM/PP composite.

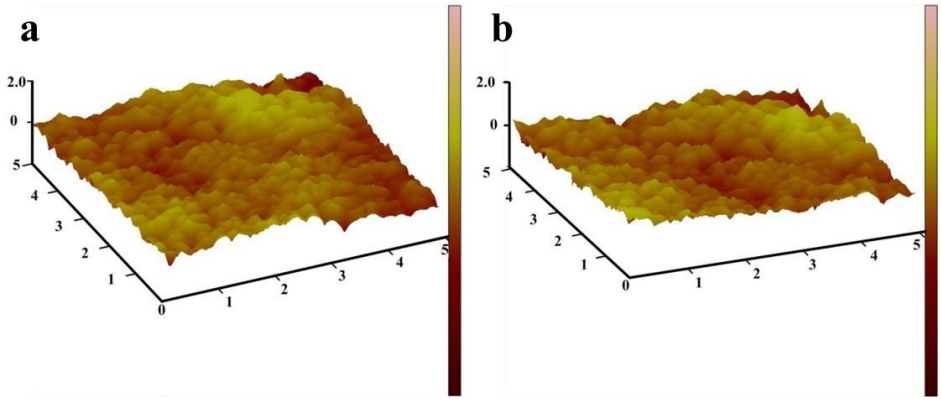

Figure S2 AFM height image (5 μm × 5 μm) images at (a) 25 °C and (b) 40 °C.

S2 Contact angle of gas bubbles in water at 25°C and 40°C

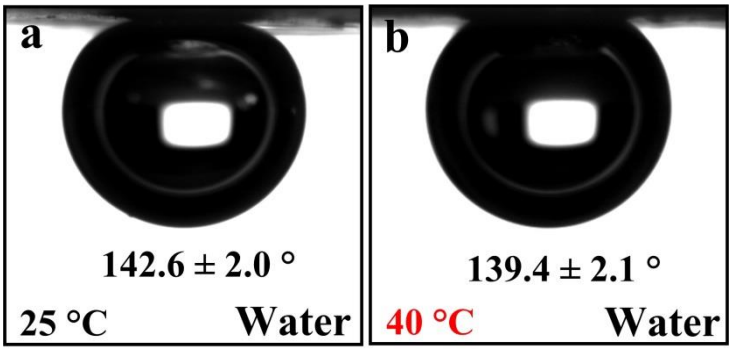

Figure S3 Contact angles of gas bubbles in water at (a) 25°C and (b) 40°C.

S3 The relationship between the contact angles of water and gas bubbles

When a solid surface is immersed in aqueous media, the water molecules are in close proximity to the solid substrate, and the gas bubbles attempting to adhere to the

substrate must compete with the intervening liquid film over the surface. As in the case of a water droplet on a solid in air, the intermolecular force between the different phases (solid/water and solid/air) would determine the behavior of a gas bubble in water. Thus, **wetting of a gas bubble on an ideal solid surface immersed in aqueous media depends on the contact angle of a sessile droplet on the same substrate in air**.[1] Water contact angle is the angle at the three-phase contact point (TPCP), where the interface tension forces reaches a balance, and it is deduced by Young's equation as follows:

$$\cos\theta_w = \frac{\gamma_{SG} - \gamma_{SL}}{\gamma_{LG}}$$

where θ_w is the water contact angle, γ_{SV} is the solid-gas interface energy, γ_{SL} is the solid-liquid interface free energy, and γ_{LV} is the liquid-gas interface energy. Gas-bubble wettability on the solid interface in aqueous media could be approximately calculated as the complementary process of liquid wettability on the solid surface. Consequently, the bubble contact angle (θ_b) at the balance point of surface-tension forces can also be derived by Young's equation as follows:

$$\cos\theta_b = \frac{\gamma_{SL} - \gamma_{SG}}{\gamma_{LG}}$$

Therefore,

$$\theta_b = 180° - \theta_w \quad (3)$$

According to Equation (3), we can approximately infer the θ_b value of an ideal solid interface in aqueous media based on the θ_w value in the air environment. The hydrophilic interface is aerophobic in aqueous media, while the hydrophobic interface is aerophilic.

However, when microstructures are introduced into interfaces with different surface energy, the relationship between **wettability of water droplets in air and** wettability **of gas bubbles in water greatly depends on the state and distribution**

of air and water in microstructures. After constructing microstructures on the interfaces with low surface energy, the interfaces achieve superhydrophobicity. If the superhydrophobic interfaces are quite water-repellent, *i.e.*, the interfaces with high θ_w (greater than 150°) and low water contact-angle hysteresis (CAH, less than 5°), the surface structures are not wetted by water during submersion. Thus, air is retained in their nano-/microstructures.[2,3] Here, CAH is defined as the difference between the cosine of the maximum and minimum static contact angles on the uphill (θ_{max}) and downhill (θ_{min}) sides upon tilting the substrate at a particular angle. As gas bubbles come into contact with these superhydrophobic interfaces, air pockets captured in the microstructure could easily coalesce with the air bubbles, then lead to air-bubble spreading. The superhydrophobic interfaces exhibit superaerophilicity with gas-bubble contact angle approaching 0°. [4-6]

A micropatterned hydrophilic/superhydrophilic interface immersed in water would possibly result in the impalement of water into roughness structures, resulting from the high capillary force.[7] Correspondingly, an air bubble brought near such a composite surface would rest on top of the asperities with water entrained beneath it. Gas bubbles retain a nearly spherical shape and are able to move around freely with a high gas-bubble contact angle approaching 180°, similar to water drops on a superhydrophobic material. Consequently, the superhydrophilic interface is superaerophobic in aqueous media.

However, θ_b was not always exactly equal to the supplementary angle of θ_w. For example, the rose petal interface exhibits superhydrophobicity with a θ_w of ~152.4°, while its θ_b is as high as 126.9°.[8] This phenomenon is mainly originates from the high water CAH of the rose petal interface. The high water CAH makes water tightly attach between the micropapillae of the rose petal interface to form absorbed islands and avoid the coalescence of adjacent air pockets around the nanofolds. Thus, the contact angle hysteresis of gas bubbles (CAH_b) manifests.

S4 AFM height image and corresponding phase image at 25°C and 40°C in water

There was no obvious morphological difference between the composite film at 25°C and 40°C. Furthermore, in the phase diagram below the LCST, we did not found distributed islands, which were separated by continuous regions, instead of the alternately bright and dark regions. When the temperature increased above the LCST, the bright and dark regions exchanged. As known, the phase images were achieved by detecting the difference of the phase angle shift between the phase angles of the signal source vibration and the actual vibration of the micro-cantilever probe. Besides of the characters of the composite interface, the interaction between the composite interface and water could also influence the phase images. Therefore, the chemical information provided by the phase images in air were more precise than that provided by the phase images in water.

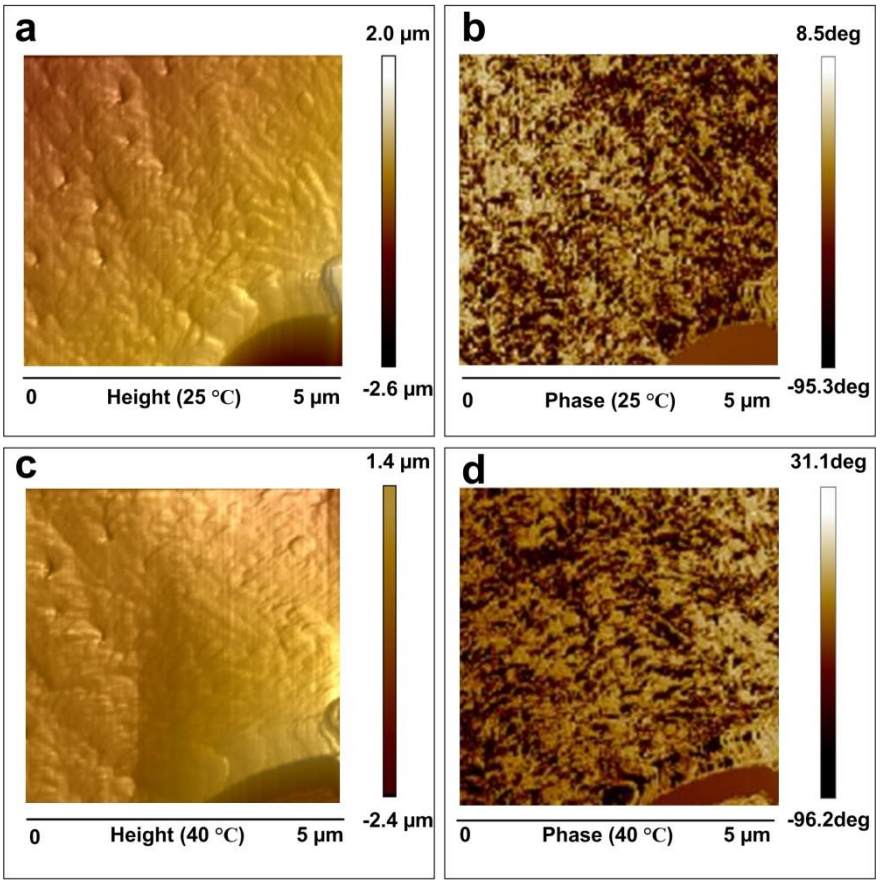

Figure S4 (a) Tapping mode AFM height image (5 μm × 5 μm) and (b) corresponding phase image at 25°C in water. (c) Tapping mode AFM height image (5 μm × 5 μm) and (d) corresponding phase image at 40°C in water.

S5 Description and explanation of the advancing and receding force curves

The receding force curves always showed a positive force data when the bubble was totally detached from the surface. We considered that these results were related to water flow during the testing process of the adhesion force. The gas bubble was fixed on a metal ring, and the force of the balance system was initially set to zero. The samples moved upward at a constant speed of 0.01 $mm \cdot s^{-1}$ until their interfaces contacted the gas bubble. With the decrease of the distance between the gas bubbles and the sample interfaces, **water was drained along the tangent direction of the gas bubble, and shear forces were introduced by water flow.**[9,10] The direction of the composition shear forces was vertically upwards. Thus, the advancing force curves showed a negative value when the gas bubble approaching to the sample surfaces. The shear forces did not disappeared until the gas bubble contacted the sample interfaces. If the sample moved up further, the vertical upward force increased gradually until it reached its maximum, and the shape of the air bubble changed from spherical to elliptical. Then the samples moved down, the receding force curves increased gradually. During the receding process, there are two forces influencing the receding force curves. They were the adhesion force between the gas bubbles and the sample interfaces, and the share forces caused by the water flow. The direction of the composition shear forces in receding process was vertically downwards. Because of the water flow toward the increasing space between the gas bubble and sample interfaces, the receding force curves showed a positive force data when the bubble was totally detached from the sample interfaces.

S6 The effect of bubble volumes on adhesion force

The bubble volume affected the adhesion force, because the bubble volume can influence the contact area of the bubbles on the composite film. The larger the contact area of the bubbles on the composite film, the larger the adhesion force. When the volume of bubble is 2 μL, the average contact area of air bubble on composite films is 0.283 ± 0.073 mm^2. The adhesion force are 30.0 ± 9.4 μN and 230.0 ± 12.3 μN at

20 °C and 40 °C, respectively (Figure S5a and b). If the volume of bubble is 1 μL, the average contact area of 1 μL bubble is 0.196 ± 0.061 mm^2, and the adhesion force decreases slightly, which are 25.0 ± 9.1 μN and 215.0 ± 9.8 μN at 20 °C and 40 °C, respectively (Figure S5c and d). Besides of the bubble volume, the distances between the bubbles and the composite films can also influence the contact area. Thus, in our experiments, in order to guarantee the contact area is same, the volume of bubble and the distance between the bubbles and the composite films were kept to be constant values.

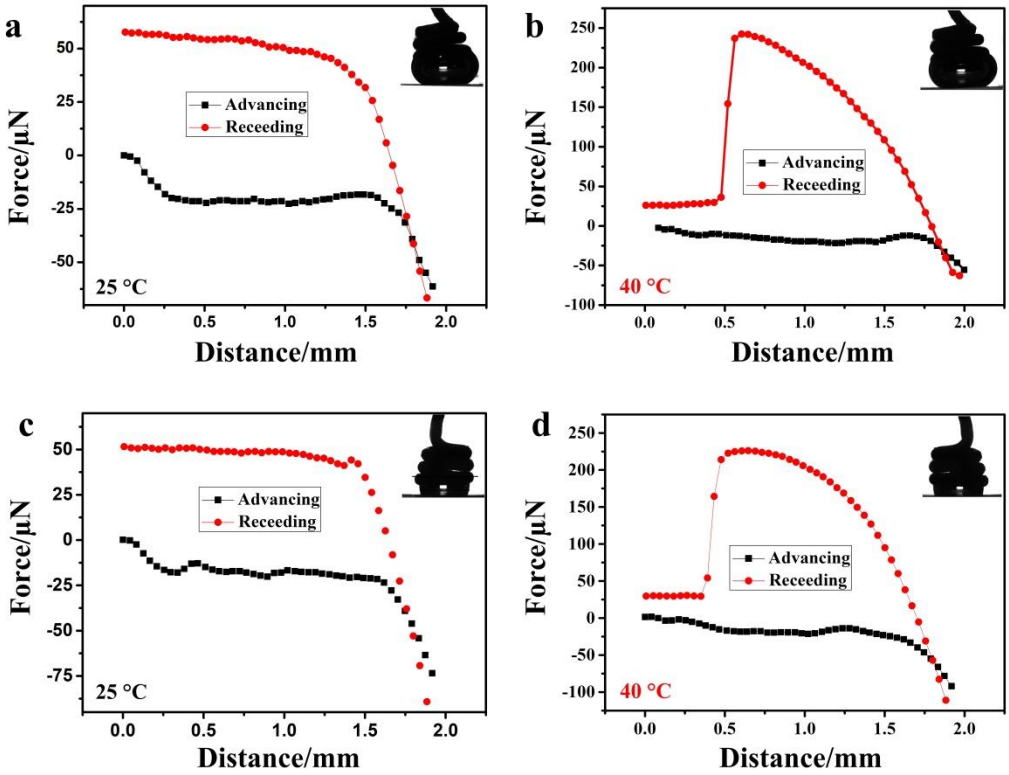

Figure S5 Force–distance curves recorded before and after 2 μL bubble contacted the PNIPAAM/PP composite film at (a) 25°C and (b) 40°C. Force–distance curves recorded before and after 1 μL bubble contacted the PNIPAAM/PP composite film at (c) 25°C and (d) 40°C.

S7 The role of PP in the polymer film

Poly (N-isopropylacrylamide), which synthesized by acrylamide or acrylic acid, can dissolve in water. Its lifetime in water is only 4-5 hours, while PP can exist stably

in water. By blending PNIPAAM and PP, **PP acted as a physical cross-linking agent**. PNIPAAM/PP composite film can achieve not only the responsiveness of air bubble adhesion and anti-adhesion, but also relatively long lifetime. Furthermore, by altering the preparation condition of the composite films, PP would help the composite films to regulate their surface morphologies and responsiveness. If PNIPAAM and PP were dissolved in dimethylbenzene at 120°C and the solvent in as-prepared uniformly blended precursor solution evaporated at 80°C, the composite film achieved island structures and thermal responsiveness (Figure S7a to c). When the dissolution temperature of PNIPAAM and PP decrease to 110 °C and the solvent evaporation temperature is room temperature, porous structures were constructed on the composite film without any thermal responsiveness (Figure S7d to f).

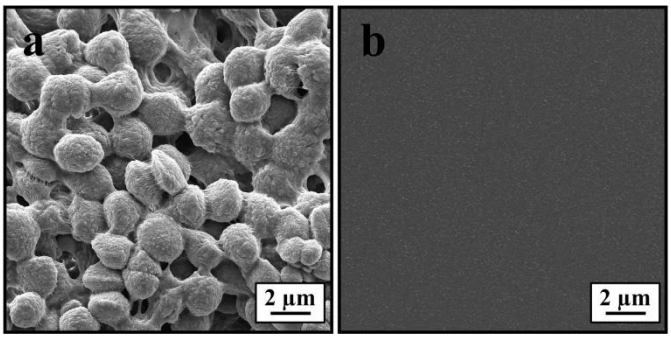

Figure S6 (a) SEM images of the surface of the PP composite. (b) SEM images of the surface of the PNIPAAM composite.

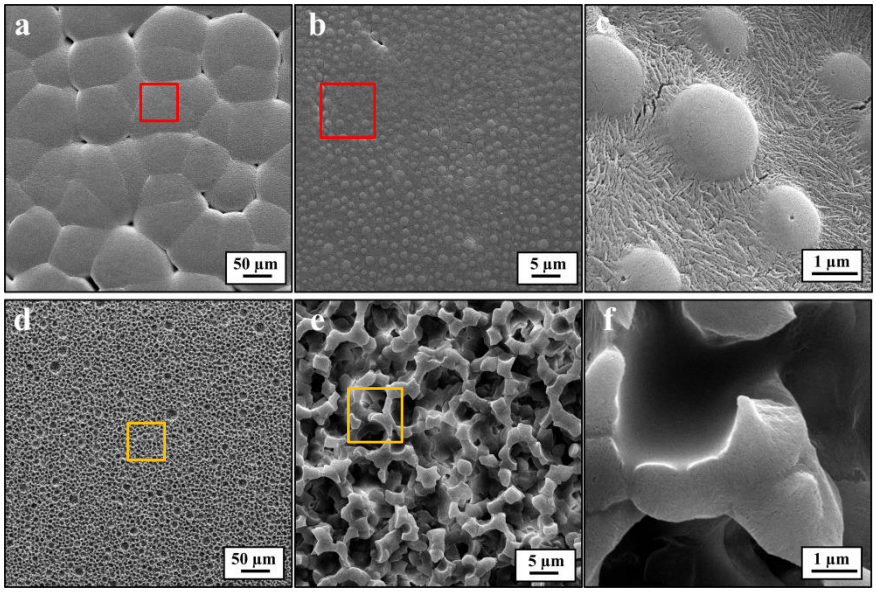

Figure S7 SEM images of PNIPAAM/PP composite films with weight ratios of 1:1 under different preparation condition. (a-c) the dissolution temperature: 120 °C, the solvent evaporation temperature: 80 °C. (d-f) the dissolution temperature: 110 °C, the solvent evaporation temperature: room temperature.

REFERENCES

[1] Zhang, P.; Wang, S.; Wang, S.; Jiang, L. Superwetting Surfaces under Different Media: Effects of Surface Topography on Wettability. Small, 2015, 11, 1939-1946.

[2] Lu, Z.; Xu, W.; Ma, J.; Li, Y.; Sun, X.; Jiang, L. Superaerophilic Carbon-Nanotube-Array Electrode for High-Performance Oxygen Reduction Reaction. Adv. Mater. 2016, 28, 7155-7161.

[3] Lei, Y.; Sun, R.; Zhang, X.; Feng, X.; Jiang, L. Oxygen-Rich Enzyme Biosensor Based on Superhydrophobic Electrode. Adv. Mater. 2016, 28, 1477-1481.

[4] Wang, J.; Zheng, Y.; Nie, F.; Zhai, J.; Jiang, L. Air Bubble Bursting Effect of Lotus Leaf. *Langmuir,* **2009**, *25,* 14129-14134.

[5] Barthlott, W.; Neinhuis, C. Purity of the sacred lotus, or escape from contamination in biological surfaces. *Planta*, **1997**, *202*, 1-8.

[6] Dorrer, C.; Rühe, J. Growth of superconducting Sm(O,F)BiS_2 single crystals. *Langmuir* **2012**, *28*, 14968.

[7] Lv, P.; Xue, Y.; Shi, Y.; Lin, H.; Duan, H. Metastable states and wetting transition of submerged superhydrophobic structures. *Phys. Rev. Lett.* **2014**, *112*, 196101.

[8] Wang, J.; Yang, Q.; Wang, M.; Jiang, L. Rose petals with a novel and steady air

bubble pinning effect in aqueous media. *Soft Matter*, **2012**, *8*, 2261-2266.

[9] Tomiyama, A.; Tamai, H.; Zun, I.; Hosokawa, S. Transverse migration of single bubbles in simple shear flows. *Chem. Eng. Sci.* **2002**, *57*, 1849-1858.

[10] Saffman, P. The lift on a small sphere in a slow shear flow. *J FLUID MECH*. **1965**, *22*, 385-400.